electricity

MDPI

Article

Techno-Economic and Reliability Assessment of Grid-Connected PV/Wind/Battery Hybrid Configurations for a Domestic District Under Unreliable Grid Conditions

Suzan Abdelhady [1,*], Ahmed Shaban [2,*] and Nasr Al-Hinai [3,*]

[1] Electrical Engineering Department, Faculty of Engineering, Fayoum University, Fayoum 63514, Egypt
[2] Department of Mechanical and Industrial Engineering, College of Engineering, Sultan Qaboos University, Al-Khoud, Muscat 123, Oman
[3] College of Engineering, A'Sharqiyah University, Ibra 400, Oman
* Correspondence: suzan.abdelhady@fayoum.edu.eg (S.A.); a.khalifa@squ.edu.om (A.S.); nasr.alhinai@asu.edu.om (N.A.-H.)

Abstract

Grid unreliability can compromise electricity supply in developing regions, yet comparative evidence on residential-district hybrid systems under consistent outage assumptions remains limited. This study compares four grid-connected architectures for a residential district in Egypt: wind/battery/grid, PV/wind/battery/grid, PV/battery/grid, and PV/wind/grid, using a simulation–optimization framework with net present cost (NPC) as the sole optimization objective. Supply adequacy, renewable fraction, grid interaction, and grid-related operational CO_2 emissions were then assessed. Under baseline conditions, PV/wind/battery/grid was the minimum-NPC hybrid configuration, with an NPC of USD 481,851, LCOE of USD 0.0711/kWh, renewable fraction of 73.8%, unserved energy of 0.306 MWh/yr, and operational CO_2 emissions of 139,533 kg/yr. Relative to grid-only supply, it reduced unserved energy by 98.5% and emissions by 65.0%, although grid-only had the lower NPC of USD 369,414. To distinguish fixed-design deterioration from adaptive redesign, baseline-optimal capacities were evaluated unchanged under a common severe grid-availability profile and compared with re-optimized counterparts. For the three battery-containing architectures with complete adaptive results, re-optimization reduced unserved energy by 73.2–97.2%, while resizing differed markedly. Among these architectures, wind/battery/grid had the lowest severe-condition NPC, only 0.63% below PV/wind/battery/grid. Deterministic ±10% sensitivity analysis retained PV/wind/battery/grid as the minimum-NPC architecture. Overall, baseline cost optimality, fixed-design transferability, and adaptation requirements are distinct, architecture-dependent planning considerations.

Keywords: hybrid renewable energy systems; grid unreliability; grid outages; optimal sizing; simulation–optimization; residential energy systems; supply adequacy; operational CO_2 emissions

Check for updates

Received: 15 April 2026
Revised: 11 August 2026
Accepted: 15 August 2026
Published: 20 August 2026

Copyright: © 2026 by the authors. Licensee MDPI, Basel, Switzerland. This article is an open access article distributed under the terms and conditions of the Creative Commons Attribution (CC BY) license.

1. Introduction

The global transition toward low-carbon electricity systems has accelerated interest in hybrid renewable energy systems (HRESs) that combine complementary energy sources with storage and grid interaction [1]. Hybridization can mitigate the variability of individual renewable energy sources, improve supply adequacy, and enhance resource utilization

when the constituent technologies exhibit complementary operating characteristics [2–4]. At the same time, the optimal design of HRESs remains a nontrivial problem because system performance depends strongly on local renewable energy resource availability [5], demand patterns [6], storage behavior [7], component costs [8], and operating strategy [9]. Recent studies and reviews have therefore identified techno-economic assessment, optimal sizing, energy management, and multi-criteria evaluation as central themes in hybrid-system design and planning [10–12].

The need for such systems becomes even more pronounced where the utility grid is present but not fully reliable [13–15]. In these contexts, energy planners are not dealing with a simple off-grid electrification problem; rather, they must design grid-connected systems that can simultaneously exploit grid availability [16], tolerate interruptions [17], reduce purchased electricity [18], and limit environmental impact [19]. Recent literature indicates that HRESs can improve supply adequacy and maintain service continuity during power interruptions, particularly in regions with favorable renewable resources but unreliable utility-grid performance [20–22]. Related research on renewable and integrated energy systems increasingly recognizes that reliability and operational flexibility should be embedded in system planning rather than treated as secondary considerations [23,24].

Within this broader field, PV–wind–battery configurations are of particular interest because solar and wind resources can exhibit complementary daily or seasonal patterns, depending on local climatic conditions, while storage can mitigate the remaining mismatch between generation and demand [25–27]. This technical complementarity, however, does not necessarily produce the lowest-cost architecture. Configuration selection must also consider resource quality, component sizing, storage utilization, grid interaction, lifecycle economics, and the adopted optimization criterion [28,29].

Despite this growing body of work, several research gaps remain. First, many published studies still focus on remote, off-grid, or sector-specific applications [30–32], while comparatively fewer studies address grid-connected district-scale domestic supply under explicit grid-unreliability conditions [33–35]. Second, a substantial portion of the literature evaluates only one or two candidate configurations, which makes it difficult to identify the comparative effect of including or excluding PV, wind, or battery storage under the same boundary conditions [36,37]. Third, although economic and environmental indicators are often reported together, the trade-off between minimum-NPC performance and operational-emissions performance is not always examined explicitly enough to support planning decisions [29,38,39]. Existing grid-connected studies in different climatic, geographical, and institutional contexts confirm the usefulness of hybrid configurations, but they also illustrate that minimum-NPC ranking and broader performance trade-offs remain strongly context-dependent [40–42].

Egypt provides a relevant case for this assessment because of its substantial solar potential, viable wind resources, growing residential electricity demand, and the importance of maintaining supply during grid interruptions [43–47]. Previous Egyptian studies have examined rural electrification, stand-alone systems, industrial applications, and large-scale renewable-energy integration. However, direct comparisons of several grid-connected PV, wind, and battery-based configurations for the same residential-district load under common technical and economic assumptions, together with controlled assessment of fixed-design performance and adaptive re-optimization under the same deteriorated grid condition, remain limited. This gap motivates an assessment that integrates lifecycle economics, supply adequacy, renewable penetration, and grid-related operational CO_2 emissions while clearly distinguishing the optimization objective from the subsequent comparative analysis. Table 1 positions the present study relative to selected research on grid-connected hybrid energy systems and unreliable-grid applications. The comparison considers application

scale, system architecture, optimization approach, treatment of grid outages, performance indicators, and sensitivity scope.

Table 1. Comparison of selected studies relevant to grid-connected hybrid energy systems and unreliable-grid applications.

Study and Application	System Configurations/ Technologies	Modeling and Optimization Approach	Grid-Outage Representation	Evaluated Indicators and Sensitivity Scope	Scope and Distinction Relative to the Present Study
[48]	PV/wind/ diesel/battery	HOMER-based optimization according to NPC and COE	Frequent blackouts were identified as an application motivation, but no alternative quantified outage scenarios were evaluated	Techno-economic assessment and greenhouse-gas emission reduction	Focused on an industrial facility and included diesel generation; did not examine a grid-connected domestic district or detailed reliability indicators
[49]	PV/battery/grid	HOMER–MATLAB framework with a predictive dispatch strategy; configurations evaluated mainly according to NPC	Daily electricity shortages were considered through dispatch and unmet-load assessment	NPC, unmet load, grid purchases, CO_2 emissions, and sensitivity to selected technical and economic parameters	Evaluated a single-house PV/battery architecture without wind generation or comparison among several representative technology architectures
[50]	PV/wind/battery system compared with conventional backup options	Grasshopper optimization with LCOE, LPSP, and payback period as decision criteria	Grid intermittency and load shedding were central to the application	Economic and reliability assessment using LCOE, LPSP, and payback period	Focused on an alternative supply solution for load shedding rather than a systematic comparison of grid-connected district-scale architectures
[51]	PV/battery/grid	HOMER-based NPC minimization using load-following and cycle-charging strategies; multi-year degradation considered	Power interruptions provided the application context, but the study did not compare multiple quantified outage-severity scenarios	Techno-economic and environmental assessment; sensitivity to solar resource, load, and battery-degradation assumptions	Restricted to a single residential PV/battery architecture and did not investigate wind integration or district-scale demand
[52]	On-grid and off-grid combinations of PV, wind, fuel cell, battery, and converter	HOMER simulation and optimization based mainly on NPC and COE	Compared grid-connected and stand-alone operation rather than explicit outage-frequency and repair-time scenarios	Economic and energy-production comparison	Focused on a remote-area application and did not provide a dedicated reliability-oriented assessment of recurrent grid interruptions
[53]	Grid-connected hybrid microgrid	HOMER-based optimization using real hourly campus load data	Load shedding was considered as an important application condition	Utility-cost savings, CO_2 reduction, ROI, and payback period	Institutional rather than domestic application; limited emphasis on comparative exclusion or inclusion of individual renewable and storage technologies

Table 1. *Cont.*

Study and Application	System Configurations/ Technologies	Modeling and Optimization Approach	Grid-Outage Representation	Evaluated Indicators and Sensitivity Scope	Scope and Distinction Relative to the Present Study
[54]	Grid-connected and stand-alone PV/vertical-axis wind/battery systems	Comparative techno-economic-environmental evaluation under different renewable-resource area allocations	Grid-connected and stand-alone modes were compared, without an explicit multi-scenario outage analysis	Economic, environmental, and technical performance	Sector-specific street-lighting application; did not address domestic district demand or quantify reliability under recurrent grid failures
[55]	Grid/diesel, grid/PV/diesel, grid/PV/diesel/battery, grid/diesel/battery, grid/PV/battery, and grid/battery	Single-objective HOMER optimization minimizing NPC subject to a zero-unmet-load requirement	Mean outage frequency of 180 outages/year, mean repair time of 2.0 h/outage, and repair-time variability of 5%	NPC, LCOE, renewable fraction, operational CO_2 emissions, grid purchases, financing sensitivity, and PV-derating sensitivity	Focused on an individual residential prosumer and PV-, diesel-, and battery-based alternatives; the study did not examine residential-district demand, wind-based architectures, or a controlled comparison of PV, wind, and storage inclusion or exclusion.
Present study: domestic district, Egypt	Wind/battery/grid, PV/wind/battery/grid, PV/battery/grid, and PV/wind/grid, benchmarked against grid-only supply	Single-objective lifecycle-cost optimization followed by comparative techno-economic, supply-adequacy, renewable-energy, and operational-emissions assessment; extended by controlled fixed-design and adaptive re-optimization analysis	Baseline and severe grid-outage conditions; the same severe grid-availability profile is used for the controlled fixed-design and adaptive analyses	Lifecycle economics, renewable contribution, grid interaction, supply adequacy, and grid-related operational CO_2 emissions; deterministic sensitivity to key technical and economic inputs	Compares alternative grid-connected hybrid architectures under common assumptions and distinguishes fixed-design deterioration from the resizing requirements, supply-adequacy effects, and lifecycle-cost implications of adaptive redesign under deteriorated grid reliability

Table 1 shows that previous studies have provided important evidence on hybrid-system feasibility, sizing, grid interaction, and outage mitigation across diverse applications. However, direct comparisons of several grid-connected PV-, wind-, and battery-based configurations for the same residential-district load under common technical and economic assumptions, together with controlled evaluation of fixed-design performance and adaptive re-optimization under the same deteriorated grid condition, remain limited. A closely related Egypt-based study examined household-scale PV-, diesel-, battery-, and grid-based alternatives under unreliable-grid conditions but did not consider district-scale demand or wind-based configurations.

Although previous studies have investigated hybrid-system sizing and performance under unreliable-grid conditions, independently re-optimizing a system for each grid condition does not reveal how a previously installed design would perform if grid reliability deteriorated while its component capacities remained unchanged. Nor does it distinguish fixed-design deterioration from the sizing and economic requirements of adaptation. This

distinction is relevant to practical planning because installed generation, storage, and conversion assets cannot generally be resized immediately in response to changes in utility-grid reliability. The present study therefore evaluates each baseline-optimal design unchanged under a common severe grid-availability profile and compares it with the corresponding architecture re-optimized under the same profile.

Accordingly, this study combines two complementary levels of analysis. First, four representative grid-connected architectures—wind/battery/grid, PV/wind/battery/grid, PV/battery/grid, and PV/wind/grid—are independently optimized and compared under common load, renewable-resource, tariff, component, and grid-outage assumptions, with grid-only supply retained as a reference benchmark. Second, a controlled severe-outage assessment compares each unchanged baseline-optimal design with the same architecture adaptively re-optimized under the same severe grid-availability profile. NPC is the sole mathematical optimization objective, while supply adequacy, renewable contribution, grid interaction, and grid-related operational CO_2 emissions are evaluated subsequently as comparative performance indicators. The principal contribution is therefore a controlled comparative assessment that distinguishes baseline minimum-NPC performance, fixed-design deterioration, and the component-sizing, supply-adequacy, and lifecycle-cost implications of adaptive redesign, rather than the development of a new optimization algorithm.

The remainder of this paper is organized as follows. Section 2 presents the modeling framework, candidate architectures, input data, economic and reliability formulations, deterministic sensitivity analysis, controlled severe-outage methodology, and verification procedures. Section 3 presents the baseline comparative results, grid-only benchmarking, and controlled severe-outage findings. Section 4 reports the deterministic tariff and input-parameter sensitivity results. Finally, Section 5 summarizes the principal findings, planning implications, limitations, and directions for future research.

2. Methodology

2.1. Modeling Approach

This study employed a simulation-based, single-objective optimization framework to evaluate grid-connected hybrid energy systems for supplying electricity to a residential district under unreliable-grid conditions. The framework was implemented using HOMER Pro 3.18.4 [56].

For each candidate architecture, the simulation–optimization model evaluated multiple combinations of PV capacity, wind-turbine units, battery units, and converter capacity, where applicable, within predefined search spaces. Each candidate design was simulated over a representative year using 8760 hourly time steps to assess its ability to supply the residential demand while satisfying the specified technical and operational constraints. These constraints included component operating limits, battery state-of-charge requirements, and grid-availability conditions.

For each feasible design, the annual technical and operating performance was incorporated into a project-lifetime economic analysis considering initial capital, component replacement, operation and maintenance, grid-purchase costs, grid-export revenues, and salvage value, where applicable. The feasible designs were ranked according to net present cost (NPC), and the minimum-NPC design was retained as the cost-optimal solution for each architecture. The optimized architecture-level solutions were subsequently compared to identify the minimum-NPC hybrid configuration under each investigated scenario.

NPC was the sole mathematical optimization objective. Supply-adequacy, renewable-energy, grid-interaction, and grid-related operational-emissions indicators were not included as simultaneous objective functions; instead, they were evaluated subsequently in the comparative assessment. The research design comprised four analytical stages:

(i) hourly time-series simulation and NPC-based optimization of each candidate architecture under baseline conditions; (ii) post-optimization comparison of lifecycle economics, supply adequacy, renewable contribution, grid interaction, and operational emissions; (iii) deterministic sensitivity analysis of selected tariff, demand, renewable-resource, and component-cost assumptions; and (iv) a controlled severe-outage assessment comparing each unchanged baseline-optimal design with the same architecture adaptively re-optimized under the same severe grid-availability profile. HOMER Pro served as the computational simulation and optimization platform, whereas the comparative and controlled assessment constituted the analytical structure of the study.

2.2. Selection of Candidate System Architectures

Four grid-connected hybrid architectures were investigated, as illustrated in Figure 1:

- Wind/battery/grid
- PV/wind/battery/grid
- PV/battery/grid
- PV/wind/grid

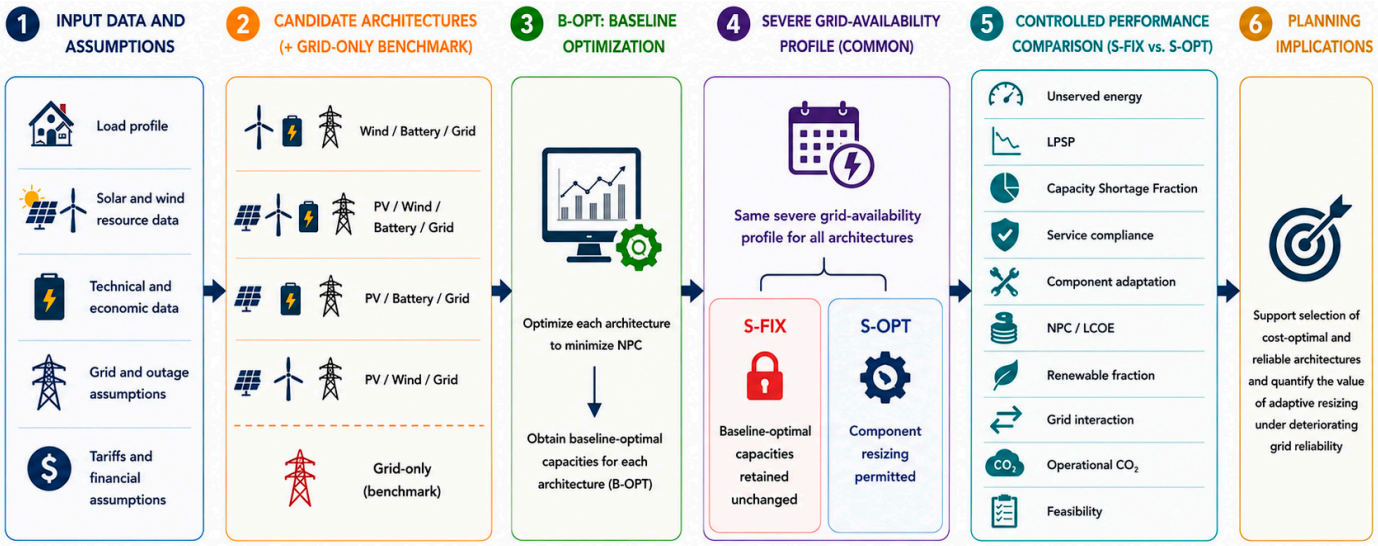

Figure 1. Simulation–optimization and controlled assessment framework for the investigated hybrid architectures.

These configurations were selected as representative architecture classes rather than as an exhaustive enumeration of all possible technology combinations. The wind/battery/grid and PV/battery/grid configurations isolate the respective contributions of wind and PV generation when supported by battery storage. The PV/wind/battery/grid configuration represents the fully integrated architecture, whereas the PV/wind/grid configuration evaluates the combined contribution of both renewable resources without battery storage.

This structured comparison enables the individual and combined effects of PV generation, wind generation, and battery storage to be examined under common load, renewable-resource, tariff, component, and outage assumptions within each scenario. Each architecture was simulated and optimized separately using its applicable component search spaces.

A grid-only system was modeled separately as a reference case for benchmarking lifecycle cost, supply adequacy, renewable contribution, and grid-related operational emissions. All four hybrid architectures were retained in the controlled severe-outage assessment. Incomplete or unavailable adaptive results, where encountered, were reported explicitly rather than being assigned numerical values.

Figure 1 summarizes the analytical workflow adopted in this study. The four candidate hybrid architectures are first optimized under the baseline grid condition using NPC as the sole objective, while grid-only supply is retained as a benchmark. The resulting baseline-optimal capacities define the reference designs for the controlled severe-condition assessment. Under the same severe grid-availability profile, S-FIX retains these capacities unchanged, whereas S-OPT permits component resizing. Comparison of S-FIX and S-OPT therefore distinguishes deterioration of the installed baseline design from the technical, economic, and supply-adequacy effects of adaptive redesign.

2.3. Input Data

The model inputs comprised: (i) the residential-district hourly electricity-demand profile; (ii) solar-irradiation and wind-speed data; (iii) the technical and economic parameters of the system components; and (iv) grid-tariff, operational-emission-factor, and outage assumptions. Common scenario-specific inputs were applied to all candidate architectures to provide a consistent basis for comparison.

2.3.1. Residential District Demand Characteristics

The case study represents a grid-connected residential district comprising 100 households. The hourly demand profile was constructed by aggregating household electricity-consumption data for 2025 obtained from utility records. The resulting profile had an annual electricity consumption of approximately 912 MWh, an average demand of 104 kW, a coincident peak demand of 530 kW, and a load factor of 0.20. Its temporal variation reflects the combined effects of household occupancy, appliance operation, and seasonal electricity use. The same baseline demand profile was applied to all candidate system configurations to ensure a consistent comparison under common boundary conditions.

2.3.2. Electrical Load

The complete hourly demand profile, comprising 8760 hourly values, was used as the electrical-load input to the simulation model. As shown in Figure 2, the profile exhibited a relatively stable base demand with recurring short-duration peaks. Summer demand was generally higher and showed more frequent peak-demand events than winter demand, reflecting increased residential cooling requirements during warmer periods.

Retaining the complete hourly profile enabled the simulation to capture seasonal variations and short-term mismatches between electricity demand and renewable generation. This hourly resolution was particularly important for evaluating renewable-energy utilization, battery charging and discharging, grid electricity purchases, unserved energy, and energy-supply performance during grid-outage periods.

2.3.3. Renewable Resource Data

Site-specific global horizontal irradiation and wind-speed data were used to estimate hourly electricity production from the PV array and wind turbines. Figure 3 presents the monthly resource characteristics. The average wind speed at 10 m height ranged from 5.32 m/s in January to 6.82 m/s in June, indicating relatively moderate seasonal variation. Solar irradiation showed a stronger seasonal pattern, increasing from approximately 3.03–3.30 kWh/m^2/day during winter to 8.40 kWh/m^2/day in June. The concurrent increase in solar irradiation and wind speed during the high-demand summer period indicates potentially favorable temporal alignment between resource availability and residential demand. The comparatively stable wind resource can also complement the more pronounced seasonal variation in solar irradiation.

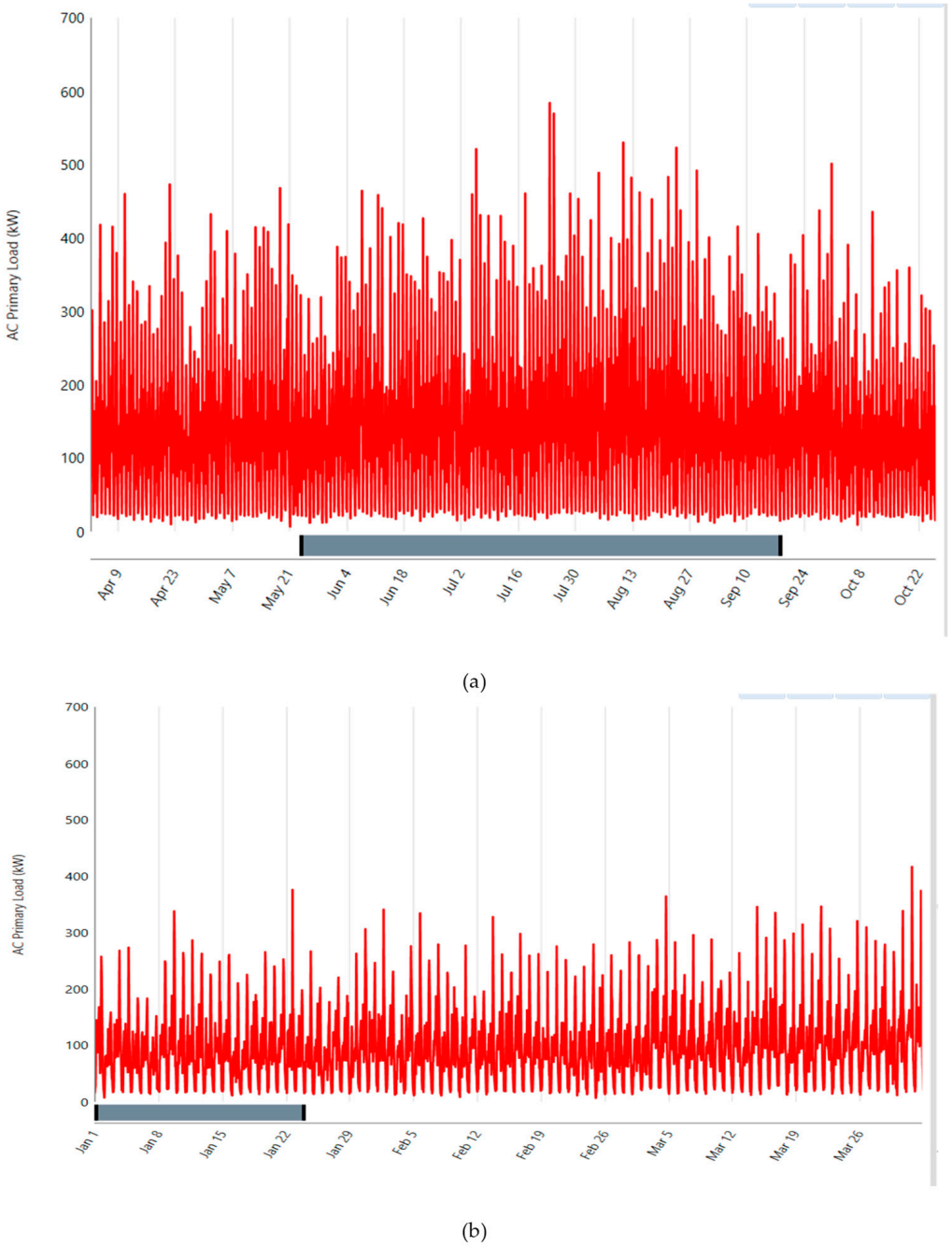

Figure 2. Hourly electricity-demand profile of the residential district during representative (**a**) summer and (**b**) winter periods.

The wind-speed data were available at a reference height of 10 m, whereas the EO20 turbine hub height is 36 m. Wind speed at hub height was therefore estimated using the power-law relationship in Equation (1):

$$V_h = V_{\text{ref}} \left(\frac{h}{h_{\text{ref}}} \right)^{\alpha} \quad (1)$$

where V_h is the wind speed at hub height h, V_{ref} is the wind speed at reference height h_{ref}, and α is the adopted wind-shear exponent.

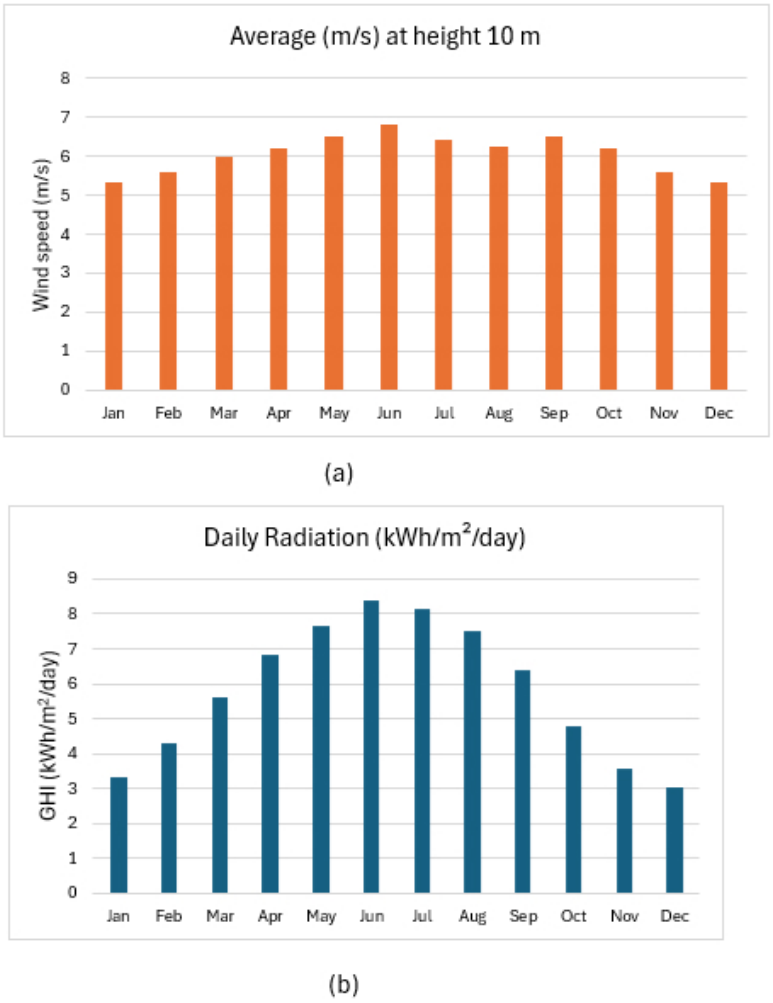

Figure 3. Monthly variation in renewable resources at the study site: (**a**) average wind speed at 10 m and (**b**) global horizontal irradiation.

2.3.4. Component Technical and Economic Parameters

Table 2 summarizes the principal technical and economic assumptions used in the component models. The PV subsystem was represented by the Suntech 325 flat plate module, with a rated output of 325 W, cell efficiency of 15%, temperature coefficient of −0.4%/K, derating factor of 85%, installation tilt angle of 30°, and service life of 25 years. The PV capital cost was assumed to be 950 $/kW.

Wind generation was modeled using the Eocycle EO20 horizontal-axis turbine. Each unit has a rated capacity of 20 kW, rotor diameter of 15.8 m, hub height of 36 m, cut-in speed of 2.7 m/s, and cut-out speed of 20 m/s. The assumed service life was 25 years, with a capital cost of 29,400 $ per turbine and an annual O&M cost of $880 per turbine.

Lead-acid batteries were adopted as the reference storage technology because of their commercial maturity, relatively low initial cost, widespread availability, and established use in cost-sensitive hybrid energy applications. Their use also provided a consistent storage assumption across the candidate architectures. The modeled battery had a minimum state of charge of 20%, maximum state of charge of 100%, and round-trip efficiency of 80%. Battery lifetime was governed by the time and/or lifetime-throughput limits represented in the adopted battery model. The reference battery therefore had a 14-year lifetime and a lifetime throughput of 800 kWh per unit, with replacement cost assumed equal to 100% of the initial battery capital cost.

Table 2. Key technical and economic parameters of the system components.

Component	Parameter	Value	Ref.
PV	Module	Suntech 325	[57]
	Type	Flat plate	
	Rated power	325 W	
	Cell efficiency	15%	
	Temperature coefficient	−0.4%/K	
	Derating factor	85%	
	Tilt angle	30°	
	Lifetime	25 years	
	Capital cost	950 $/kW	
	O&M cost	23 $/kW/yr	
Wind turbine	Model	Eocycle EO20	[57]
	Axis type	Horizontal axis	
	Rated power	20 kW/unit	
	Rotor diameter	15.8 m	
	Hub height	36 m	
	Cut-in wind speed	2.7 m/s	
	Cut-out wind speed	20 m/s	
	Lifetime	25 years	
	Capital cost	29,400 $/turbine	
	O&M cost	880 $/turbine/year	
Battery	Chemistry	Lead-acid	
	Capital cost	105 $/kWh	[55,58]
	Lifetime	14 years	
	Lifetime throughput	800 kWh	
	Replacement cost	100% of capital cost	
	Minimum state of charge	20%	
	Maximum state of charge	100%	
	Round-trip efficiency	80%	
	O&M cost	8 $/unit/year	
Converter	Efficiency	95%	[59]
	Lifetime	15 years	
	Capital cost	290 $/kW	
	Replacement cost	100% of capital cost	
Grid	Purchase price	0.078 $/kWh	[60]
	Sellback price	0.014 $/kWh	[60]
	Operational emission factor	0.447 kg CO_2/kWh	[44]
	Nominal discount rate	28.25%	[55,61]
	Inflation rate	9.4%	[55,61]

The use of lead-acid storage should not be interpreted as evidence of superiority over modern battery technologies. Lithium-ion batteries generally offer higher round-trip efficiency, greater usable depth of discharge, higher energy density, and longer cycle life, although usually with a higher initial cost. The influence of alternative battery chemistries on system sizing, replacement requirements, lifecycle cost, and environmental performance is therefore identified as an important extension of the present analysis.

The converter was modeled with an efficiency of 95% and a lifetime of 15 years. All capital, replacement, and O&M costs were applied consistently across the candidate architectures.

2.3.5. Grid Representation and Outage Scenarios

The utility grid was modeled as a supplementary electricity source and, where surplus renewable electricity was available, as an export sink. The assumed purchase tariff was \$0.078/kWh, while the sellback tariff was \$0.014/kWh (Table 2). The large difference between these tariffs favors local consumption of renewable electricity rather than oversizing the system primarily for grid export.

Two grid-outage conditions were considered (see Table 3). The baseline condition represents the moderate periodic interruptions originally assumed in the study, whereas the severe condition was adapted from Ref. [55] and was parameterized using a mean outage frequency of 180 outages/year, a mean repair time of 2.0 h, and repair-time variability of 5%. For the controlled severe-outage assessment, one hourly grid-availability profile generated under these assumptions was fixed and reused across paired S-FIX and S-OPT simulations. This ensured that differences between the paired cases reflected component resizing rather than differences in outage occurrence and timing.

Table 3. Grid-availability and outage scenarios considered in the analysis.

Scenario	Grid Outage Characteristics	Interpretation	Source
Baseline scenario	One hour of outage during weekends in winter and two hours of outage during weekends in summer	Represents the original moderate grid unreliability condition considered in the base analysis	Assumed baseline scenario
Severe scenario	Mean outage frequency of 180 outages/year, mean repair time of 2.0 h per outage, and repair time variability of 5%	Used for the controlled fixed-design and adaptive assessment under substantially degraded grid reliability.	Adapted from [55]

2.4. Optimization Criterion and Economic Assessment Indicators

The candidate systems were optimized by minimizing the net present cost (NPC) over the project lifetime. NPC represents the present value of the initial capital cost and all subsequent operation and maintenance, replacement, and grid-electricity purchase costs, less revenues from electricity exported to the grid and the terminal salvage value, where applicable:

$$NPC = C_{\mathrm{cap},0} + \sum_{t=1}^{T} \frac{C_{\mathrm{O\&M},t} + C_{\mathrm{rep},t} + C_{\mathrm{grid,pur},t} - R_{\mathrm{grid,sale},t}}{(1+i)^t} - \frac{S_T}{(1+i)^T} \quad (2)$$

where $C_{\mathrm{cap},0}$ is the initial capital cost of the applicable system components, including the PV array, wind turbines, battery bank, and converter; $C_{\mathrm{O\&M},t}$ is the operation and maintenance cost in year t; $C_{\mathrm{rep},t}$ is the replacement cost incurred in year t; $C_{\mathrm{grid,pur},t}$ is the cost of electricity purchased from the grid in year t; $R_{\mathrm{grid,sale},t}$ is the revenue from electricity exported to the grid in year t; S_T is the total salvage value of the system components at the

end of the project lifetime; i is the real discount rate; T is the project lifetime; and t is the year index. The project lifetime was set to 25 years.

The real discount rate can be calculated from the nominal discount rate as follows:

$$i = \frac{i^* - f}{1+f} \tag{3}$$

where i^* is the nominal discount rate, and f is the inflation rate.

The levelized cost of energy was used as a complementary economic indicator:

$$LCOE = \frac{C_{\text{ann,tot}}}{E_{\text{served}}} \tag{4}$$

where E_{served} is the total annual electrical energy served, including electricity supplied to the residential load and electricity sold to the grid.

$$C_{\text{ann,tot}} = CRF(i,T).NPC \tag{5}$$

where $C_{\text{ann,tot}}$ is the total annualized cost, and CRF is the capital recovery factor:

$$CRF(i,T) = \frac{i(1+i)^T}{(1+i)^T - 1} \tag{6}$$

2.5. Reliability Assessment

Supply adequacy was assessed using annual unserved energy, loss-of-power-supply probability (LPSP), and energy-supply availability. Annual unserved energy was calculated as:

$$E_{uns} = \sum_{t=1}^{8760} P_{uns,t}.\Delta t \tag{7}$$

where $P_{uns,t}$ is the unserved electrical demand during time step t, and $.\Delta t$ is the simulation time step, equal to 1 h in the present analysis.

Loss-of-power-supply probability was calculated as:

$$LPSP = \frac{E_{uns}}{E_{\text{load}}} \tag{8}$$

where E_{load} is the annual electricity demand. The corresponding energy supply availability was expressed as:

$$A_E(\%) = 100(1 - LPSP) \tag{9}$$

Capacity Shortage Fraction (CSF), as reported by the simulation model, was additionally used to characterize the annual capacity shortage relative to the electrical demand.

2.6. Environmental Assessment

The quantified environmental assessment was limited to operational CO_2 emissions, primarily those associated with electricity imported from the grid. Annual operational emissions were estimated as:

$$CO_{2,\text{op}} = E_{\text{grid}} \times EF_{\text{grid}} \tag{10}$$

where E_{grid} is annual grid electricity consumption and EF_{grid} is the grid emission factor of 0.447 kg CO_2/kWh.

This metric enabled a consistent comparison of the operational carbon burden of the candidate configurations. However, it does not include embodied emissions associated with raw-material extraction, component manufacturing, transportation, replacement, or

end-of-life treatment. Future work should therefore integrate a full life-cycle assessment to evaluate the overall environmental performance of the alternative hybrid configurations.

2.7. Sensitivity and Scenario Analysis

A deterministic sensitivity analysis was conducted to evaluate the local stability of the minimum-NPC solutions under variations in selected economic and technical inputs. The analysis comprised two components: electricity-tariff sensitivity and one-at-a-time variation of selected technical and economic parameters.

First, the effects of the grid electricity purchase price and grid sellback tariff on the net present cost were examined. These parameters were selected because they directly influence the cost of imported electricity and the financial value of surplus renewable energy exported to the grid. For each tariff combination, the system was re-optimized and the resulting NPC and minimum-NPC architecture were recorded.

Second, the sensitivity analysis was extended to the principal uncertain technical and economic inputs, namely:

- annual electricity demand;
- solar irradiation;
- wind speed; and
- component initial capital cost.

Each parameter was varied independently by −10% and +10% relative to its baseline value, while all other inputs were maintained at their reference levels. The optimization was repeated for every sensitivity case to determine whether changes in the input assumptions affected the minimum NPC architecture and its optimal component sizes. The resulting configurations were compared in terms of PV capacity, number of wind turbines, battery capacity, NPC, LCOE, annual operating cost, initial capital requirement, renewable fraction, grid electricity purchase, annual unserved energy, loss-of-power-supply probability, energy-supply availability, and operational CO_2 emissions.

These one-at-a-time variations were used to evaluate the local stability of the minimum-NPC architecture and associated sizing and economic outcomes within the investigated deterministic ranges. They do not constitute a probabilistic or multi-year uncertainty assessment.

2.8. Controlled Severe-Outage Assessment Method

Scenario-specific re-optimization identifies a design appropriate to a specified grid-reliability condition but does not show how a system originally optimized under the baseline condition would perform if grid reliability subsequently deteriorated while its installed capacities remained unchanged. A controlled severe-outage assessment was therefore conducted for all four hybrid architectures.

Three analytical states were distinguished. B-OPT denotes the baseline-optimal design and provides the installed reference capacities. In the fixed-design severe case (S-FIX), these capacities were retained unchanged while the system was evaluated under the common severe grid-availability profile. In the adaptive severe case (S-OPT), the same architecture was re-optimized under the same profile, permitting component resizing within the specified search space.

All non-sizing inputs were held constant between paired S-FIX and S-OPT cases, including load, solar and wind resources, tariffs, component characteristics and costs, financial parameters, dispatch settings, battery assumptions, operating-reserve settings, and the grid-emission factor. The controlled distinction was therefore whether component resizing was prohibited or permitted.

For each case, component capacities, annual unserved energy, LPSP, energy-supply availability, capacity shortage fraction (CSF), grid interaction, renewable fraction, NPC, LCOE, and grid-related operational CO_2 emissions were recorded.

2.9. Model Verification and Benchmark Comparison

Selected annual unserved-energy, LPSP, energy-supply-availability, and grid-related operational-emissions outputs were independently recalculated using the governing relationships to verify their numerical consistency. In addition, the severe PV/battery/grid result was compared quantitatively with the published residential Grid/PV/Battery case reported in Ref. [55]. The reference provides a relevant cross-study benchmark because it considers a residential application in Egypt under the same nominal severe grid-outage parameters. However, the studies differ substantially in load scale, tariff structure, component sizing and costs, resource and demand profiles, and service-level requirements. Accordingly, the comparison is used as a published reasonableness benchmark rather than as direct validation.

3. Results and Discussion

3.1. Baseline Scenario Optimization and Comparative Performance

Table 4 summarizes the techno-economic, supply-adequacy, renewable-energy, grid-interaction, and grid-related operational-emissions performance of the four hybrid architectures under the baseline grid-outage scenario. Each architecture was optimized separately by minimizing net present cost. The remaining indicators were used in the subsequent comparative assessment. Accordingly, the configuration with the lowest NPC is interpreted as the minimum NPC hybrid architecture rather than as a multi-objective optimum or a universally preferred solution.

Table 4. Techno-economic, reliability, and operational environmental performance under the baseline outage scenario.

Configuration	PV (kW)	EO20 Turbines	1 kWh LA Batteries	Grid Purchase (kWh/yr)	NPC ($)	LCOE ($/kWh)	Operating Cost ($/yr)	Initial Capital ($)	Renewable Fraction (%)	Annual Unserved Energy (MWh/yr)	LPSP	Energy-Supply Availability (%)	Operational CO_2 (kg/yr)
PV/wind/battery/grid	9.33	9	601	312,154	481,851	0.0711	17,379	376,510	73.8	0.306	0.00033534	99.9664658	139,533
Wind/battery/grid	—	9	842	319,410	539,598	0.0803	21,210	418,817	72.9	0	0	100	142,776
PV/battery/grid	199	—	761	582,635	642,979	0.12	55,877	302,992	38.3	0.377	0.00041315	99.9586849	260,438
PV/wind/grid	2731	102	—	69,868	5,810,000	0.0943	16,095	5,720,000	99.4	0.0994	0.00010893	99.9891068	31,231

Among the investigated hybrid systems, the PV/wind/battery/grid configuration achieved the lowest NPC of $481,851 and the lowest levelized cost of energy (LCOE) of $0.0711/kWh. The optimized configuration comprised 9.33 kW of PV capacity, nine 20 kW EO20 wind turbines, and 601 lead-acid battery units. It also recorded an annual operating cost of $17,379, a renewable fraction of 73.8%, grid electricity purchases of 312,154 kWh/yr, and operational CO_2 emissions of 139,533 kg/yr.

Relative to the independently optimized wind/battery/grid configuration, the PV/wind/battery/grid solution achieved a 10.7% lower NPC, an 11.5% lower LCOE, an 18.1% lower annual operating cost, and a 28.6% lower battery requirement. Grid purchases and operational CO_2 emissions also decreased by approximately 2.3%, while the renewable fraction increased from 72.9% to 73.8%. Under the adopted assumptions, these results indicate that even a relatively small PV contribution can improve the economic balance of a

wind-dominated system by reducing storage requirements and partially complementing wind generation.

The wind/battery/grid configuration achieved zero reported annual unserved energy under the baseline scenario and maintained a renewable fraction of 72.9%. However, its larger storage requirement of 842 battery units increased its initial capital cost to $418,817 and its NPC to $539,598. The configuration achieving zero reported unserved energy did not coincide with the minimum-NPC hybrid solution.

The PV/battery/grid configuration exhibited the least favorable lifecycle and operational performance among the storage-based alternatives. Despite including 199 kW of PV capacity and 761 battery units, it required 582,635 kWh/yr of grid electricity, corresponding to the lowest renewable fraction of 38.3% and the highest operational CO_2 emissions of 260,438 kg/yr. Its NPC of $642,979, LCOE of $0.120/kWh, and annual operating cost of $55,877 were also the highest among the first three configurations. Relative to the cost-optimal PV/wind/battery/grid system, its NPC was approximately 33.4% higher, while its grid purchases and operational emissions were approximately 86.7% higher. This finding highlights the importance of the wind resource at the study location and shows that the relatively low initial capital cost of the PV/battery/grid architecture does not translate into favorable lifecycle economics.

The PV/wind/grid configuration achieved the highest renewable fraction of 99.4%, the lowest grid purchase of 69,868 kWh/yr, and the lowest operational CO_2 emissions of 31,231 kg/yr. However, these benefits required 2731 kW of PV capacity and 102 EO20 wind turbines, resulting in an initial capital cost of $5.72 million and an NPC of $5.81 million. Its NPC was approximately twelve times that of the cost-optimal hybrid system. Consequently, a very high renewable fraction was obtained, but only through substantial generation oversizing and a disproportionately high capital and lifecycle cost.

The large renewable capacities of the PV/wind/grid architecture warrant additional interpretation. The optimized system contains approximately 2.731 MW of PV and 2.040 MW of wind capacity, giving a combined renewable nameplate capacity of approximately 4.77 MW. In the absence of battery storage, surplus renewable production cannot be shifted temporally from periods of high generation to later periods of high demand or grid interruption, and the optimizer therefore compensates partly through generation oversizing. Moreover, the present model does not impose explicit land-area, siting-density, maximum-renewable-capacity, or grid-export constraints. Accordingly, the PV/wind/grid result should be interpreted as an unconstrained system-level optimization outcome rather than as a site-validated implementation design.

Overall, the baseline results show that the relative performance of the investigated architectures depends on the evaluation criterion. The PV/wind/battery/grid system achieved the lowest NPC among the hybrid alternatives, whereas wind/battery/grid provided the highest supply adequacy and PV/wind/grid delivered the highest renewable fraction and lowest grid-related operational emissions, but at a disproportionately high capital and lifecycle cost. The PV/battery/grid configuration performed least favorably across most lifecycle and operating indicators. These findings confirm that no single architecture is superior across all criteria and that system selection requires an explicit trade-off among cost, reliability, renewable contribution, and emissions.

3.2. Reliability Assessment Under the Baseline Outage Scenario

The reliability indicators show that all four hybrid configurations maintained high energy-supply adequacy under the baseline outage scenario. Nevertheless, measurable differences exist among the architectures and should not be obscured by describing all unserved-energy values as simply negligible.

The wind/battery/grid system achieved zero reported annual unserved energy and an energy-supply availability of 100%. This result was associated with its relatively large battery bank of 842 units, although the larger storage requirement was associated with both initial and lifecycle costs. The PV/wind/grid configuration also demonstrated very high supply adequacy, with annual unserved energy of 0.0994 MWh/yr, an LPSP of 0.00010893, and energy-supply availability of approximately 99.9891%. In this case, high supply adequacy was achieved through substantial renewable-generation oversizing rather than battery storage.

The minimum-NPC hybrid configuration recorded annual unserved energy of 0.306 MWh/yr and an LPSP of 0.00033534, corresponding to energy-supply availability of approximately 99.9665%. Its unserved-energy fraction represented approximately 0.0335% of annual demand while requiring substantially lower lifecycle expenditure than the wind/battery/grid and PV/wind/grid alternatives.

The PV/battery/grid configuration recorded the highest annual unserved energy among the hybrid architectures, at approximately 0.377 MWh/yr, with an LPSP of 0.00041315 and energy-supply availability of approximately 99.9587%. Its weaker reliability performance was accompanied by higher grid dependence, higher operating cost, and higher operational emissions. This suggests that, under the studied resource and demand conditions, the absence of wind generation was associated with less favorable performance.

The baseline reliability results therefore demonstrate that high supply adequacy can be achieved through different design strategies, including greater storage capacity, complementary renewable generation supported by storage, or extensive renewable-generation oversizing. These alternatives have markedly different lifecycle-cost and practical implications; therefore, maximum supply adequacy does not necessarily coincide with minimum NPC.

3.3. Trade-Off Between Lifecycle Cost, Renewable Fraction, and Grid-Related Operational CO_2 Emissions

Figure 4 compares renewable fraction and grid-related operational CO_2 emissions across the optimized hybrid architectures, with the corresponding NPC values annotated for each configuration. Relative to the minimum-NPC PV/wind/battery/grid configuration, the PV/wind/grid system reduced grid-related operational emissions by approximately 77.6% and increased the renewable fraction from 73.8% to 99.4%. However, its NPC increased from approximately \$0.482 million to \$5.81 million, representing an approximately twelvefold lifecycle-cost increase.

This comparison reveals a substantial cost premium associated with achieving a very high renewable fraction. It represents a post-optimization assessment rather than a formal multi-objective or Pareto-front analysis: NPC was the sole optimization objective, while renewable fraction and operational emissions were used to interpret the broader consequences of the independently optimized architectures. Accordingly, PV/wind/battery/grid remained the minimum-NPC hybrid configuration, whereas PV/wind/grid achieved the highest renewable fraction and lowest grid-related operational emissions.

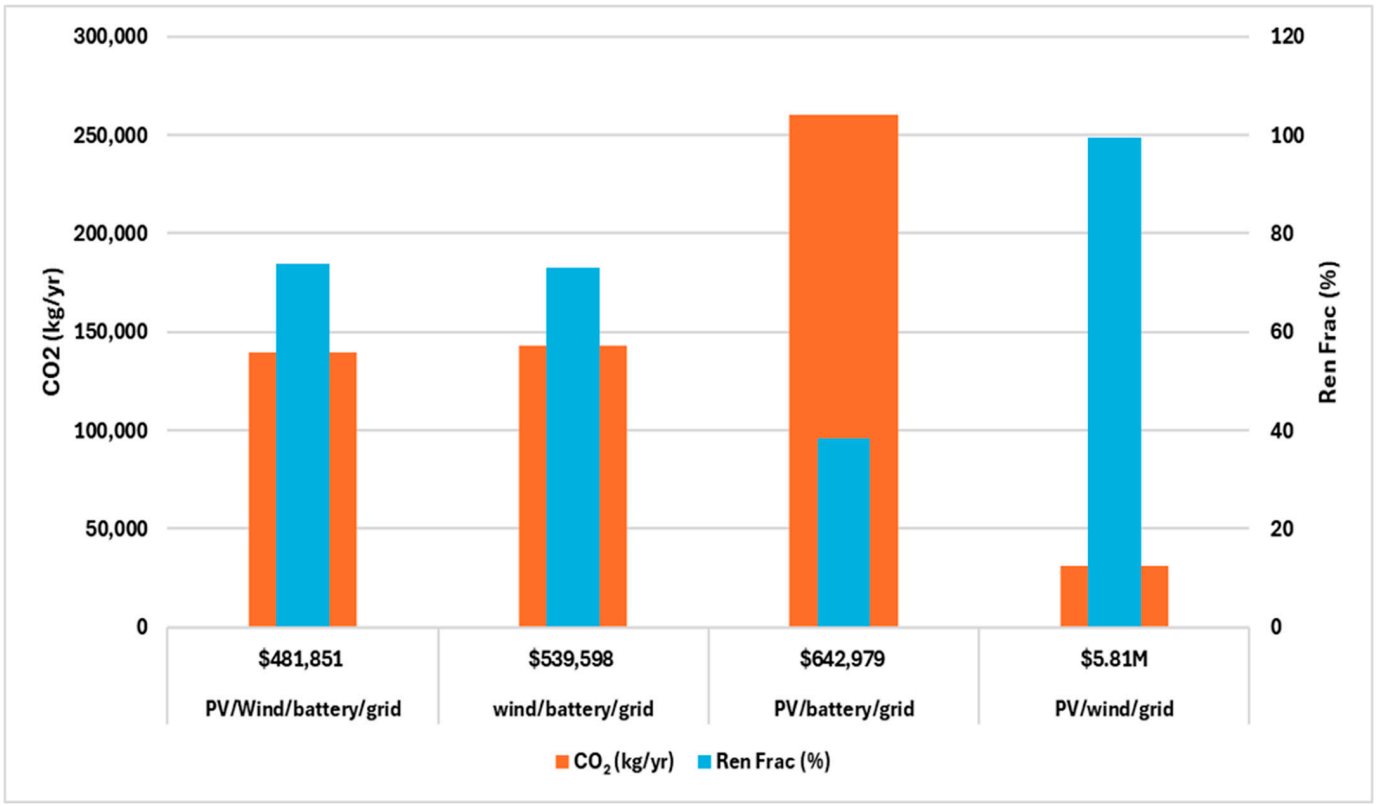

Figure 4. Renewable fraction and grid-related operational CO_2 emissions of the four independently NPC-optimized hybrid architectures under the baseline outage condition.

3.4. Benchmarking the Minimum Hybrid Configuration Against Grid-Only Supply

Table 5 compares the grid-only base case with the cost-optimal PV/wind/battery/grid configuration. The grid-only system achieved a lower NPC of $369,414, compared with $481,851 for the hybrid system. Thus, hybridization imposed an additional lifecycle cost of $112,437, equivalent to an NPC premium of approximately 30.4%.

Table 5. Comparison of grid-only supply and the cost-optimal hybrid configuration.

Indicator	Grid-Only Base Case	PV/Wind/Battery/Grid	Change
NPC ($)	369,414	481,851	+30.4%
Annual unserved energy (MWh/yr)	20.000	0.306	−98.5%
LPSP	0.02193	0.00033534	−98.5%
Energy-supply availability (%)	97.807	99.9665	+2.16 percentage points
Operational CO_2 emissions (kg/yr)	398,929	139,533	−65.0%

This additional expenditure produced substantial reliability and operational environmental benefits. The grid-only system recorded annual unserved energy of approximately 20 MWh/yr, corresponding to an LPSP of approximately 0.0219 and energy-supply availability of 97.807%. The hybrid system reduced annual unserved energy to 0.306 MWh/yr, representing a reduction of approximately 98.5%, while increasing energy-supply availability to approximately 99.9665%.

Annual operational CO_2 emissions also decreased from 398,929 kg/yr for grid-only supply to 139,533 kg/yr for the hybrid system, corresponding to a reduction of approximately 65.0%. The reduction follows directly from the lower dependence on grid electricity and the contribution of local renewable generation.

The grid-only case is therefore the least-cost option in strictly monetary terms, whereas the PV/wind/battery/grid configuration provides substantially higher supply adequacy and lower operational emissions at a higher lifecycle cost. The planning choice therefore depends on whether the decision criterion is restricted to lifecycle monetary cost or also considers the value of improved supply adequacy and lower grid-related operational emissions. No formal weighting of these attributes was undertaken.

Overall, the grid-only system remained the least-cost option, while the minimum-NPC PV/wind/battery/grid configuration required a 30.4% higher NPC to reduce unserved energy by approximately 98.5% and grid-related operational CO_2 emissions by 65.0%. The hybrid configuration should therefore be viewed as an investment in improved supply adequacy and lower operational emissions rather than as a direct cost-saving option.

3.5. Controlled Fixed-Design and Adaptive Assessment Under Severe Grid Outages

The controlled severe-outage assessment compares the baseline-optimal designs operated without resizing (S-FIX) with the corresponding architectures re-optimized under the same severe grid-availability profile (S-OPT). Because the operating conditions and non-sizing assumptions were maintained between each paired case, the comparison distinguishes deterioration of the installed baseline design from the effects and requirements of adaptive resizing. The loss-of-power-supply probability (LPSP), energy-supply availability, and capacity shortage fraction (CSF) characterize supply adequacy. In Tables 6–8, an em dash indicates that a technology is not included in the corresponding architecture, whereas N/A indicates that no complete numerical S-OPT result is available.

Table 6. Component sizing and supply-adequacy results under the controlled severe grid condition.

Configuration	Case	PV (kW)	EO20 Turbines (No.)	1 kWh Lead-Acid Batteries (No.)	Converter (kW)	Annual Unserved Energy (MWh/yr)	LPSP	Energy-Supply Availability (%)	CSF (%)
Wind/battery/grid	S-FIX	—	9	842	215	10.032	0.01100	98.90	2.240
Wind/battery/grid	S-OPT	—	9	878	218	0.281	0.00031	99.97	0.100
PV/wind/battery/grid	S-FIX	9.33	9	601	147	1.012	0.00111	99.89	0.275
PV/wind/battery/grid	S-OPT	9.78	9	884	217	0.271	0.00030	99.97	0.098
PV/battery/grid	S-FIX	199	—	761	192	3.466	0.00380	99.62	0.517
PV/battery/grid	S-OPT	237	—	1117	275	0.472	0.00052	99.95	0.100
PV/wind/grid	S-FIX	2731	102	—	286	2.253	0.00247	99.75	0.357
PV/wind/grid	S-OPT	N/A	N/A	N/A	N/A	N/A	N/A	N/A	N/A

Table 7. Economic, grid-interaction, renewable-energy, and grid-related operational-emissions results under the controlled severe grid condition.

Configuration	Case	Grid Purchases (kWh/yr)	Grid Sales (kWh/yr)	NPC (USD)	LCOE (USD/kWh)	Renewable Fraction (%)	Grid-Related Operational CO_2 Emissions (kg/yr)
Wind/battery/grid	S-FIX	315,094	267,589	470,756	0.0707	73.1	140,847
Wind/battery/grid	S-OPT	315,094	255,652	549,996	0.0827	73	140,847
PV/wind/battery/grid	S-FIX	307,973	266,336	485,218	0.0723	73.9	137,664
PV/wind/battery/grid	S-OPT	307,643	265,864	553,469	0.0825	73.9	137,516
PV/battery/grid	S-FIX	576,194	26,680	642,542	0.121	38.4	257,559
PV/battery/grid	S-OPT	551,408	65,652	738,797	0.133	43.6	246,479
PV/wind/grid	S-FIX	78,534	8,949,088	5,820,000	0.104	99.2	35,105
PV/wind/grid	S-OPT	N/A	N/A	N/A	N/A	N/A	N/A

Table 8. Relative changes from S-FIX to S-OPT for the battery-containing architectures.

Configuration	Unserved-Energy Reduction (%)	CSF Reduction (%)	PV-Capacity Change (%)	Battery-Bank Size Change (%)	Converter-Capacity Change (%)	NPC Change (%)
Wind/battery/grid	97.2	95.6	—	4.3	1.4	16.8
PV/wind/battery/grid	73.2	64.3	4.8	47.1	47.6	14.1
PV/battery/grid	86.4	80.7	19.1	46.8	43.2	15

3.5.1. Fixed-Design Performance Under Severe Grid Conditions

The S-FIX results reveal substantial differences in how the baseline-optimal designs respond to deteriorated grid reliability. Wind/battery/grid experienced the largest supply shortfall, with annual unserved energy reaching 10.032 MWh/yr, whereas PV/wind/battery/grid limited the shortfall to 1.012 MWh/yr. PV/battery/grid and PV/wind/grid exhibited intermediate values of 3.466 and 2.253 MWh/yr, respectively, with the remaining supply-adequacy indicators showing the same general pattern.

This comparison demonstrates that baseline performance does not directly predict fixed-design performance under more severe grid conditions. Wind/battery/grid reported zero unserved energy under the baseline condition but experienced the greatest deterioration when its installed capacities were retained. In contrast, PV/wind/battery/grid exhibited the strongest fixed-design supply adequacy under the severe grid condition. Baseline minimum-NPC performance and fixed-design transferability should therefore be regarded as distinct characteristics.

The PV/wind/grid result provides additional insight into the role of storage. Despite its very large renewable-generation capacity, the configuration experienced non-zero unserved energy while exporting approximately 8.95 GWh/yr, equivalent to about 9.8 times the annual district electricity demand. The coexistence of substantial surplus generation and supply shortfalls indicates that high annual renewable production alone does not ensure supply adequacy. In the absence of storage, surplus generation cannot be shifted to periods when grid interruptions coincide with insufficient renewable production. This result reinforces the importance of temporal matching among renewable generation, demand, storage, and grid availability rather than relying on annual energy balance alone.

Overall, the S-FIX analysis shows that evaluating only the baseline-optimal solution provides incomplete information about how an installed architecture may perform if grid reliability subsequently deteriorates.

3.5.2. Adaptive Re-Optimization Under the Severe Grid Condition

Adaptive re-optimization substantially improved supply adequacy for all three battery-containing architectures, but the physical changes required to achieve this improvement differed markedly. Table 7 presents the corresponding economic, grid-interaction, renewable-energy, and grid-related operational-emissions results. For S-FIX, NPC represents the lifecycle-cost outcome of operating the unchanged baseline design under the severe grid condition and is therefore not a severe-condition optimum.

Wind/battery/grid provides the clearest example of the distinction between deterioration and adaptation. Although it experienced the largest S-FIX supply shortfall, its S-OPT design required only modest increases in battery and converter capacities, while the number of wind turbines remained unchanged. Conversely, PV/wind/battery/grid exhibited much stronger fixed-design supply adequacy but required substantial increases in storage and converter capacities when re-optimized. PV/battery/grid required broader adaptation involving additional PV generation together with substantial increases in battery and converter capacities.

These contrasting responses demonstrate that the magnitude of fixed-design deterioration does not determine the extent of subsequent redesign. An architecture can deteriorate substantially while requiring relatively limited physical modification, whereas another can retain stronger fixed-design performance but require considerably greater resizing when optimized specifically for the severe condition.

The economic results further show that the two wind-containing S-OPT architectures were closely matched. Among the three architectures with complete S-OPT results, wind/battery/grid achieved the lowest NPC at USD 549,996, while PV/wind/battery/grid was only approximately 0.63% higher at USD 553,469. PV/wind/battery/grid nevertheless provided marginally lower unserved energy, a slightly higher renewable fraction, and lower grid-related operational CO_2 emissions. Given the small NPC difference, these results indicate a near-cost comparison with different secondary performance characteristics rather than a clear overall advantage for either architecture.

PV/battery/grid exhibited a markedly higher NPC than the two wind-containing S-OPT configurations and remained more dependent on grid electricity. Although adaptive resizing increased its renewable fraction and reduced both grid purchases and grid-related operational CO_2 emissions, its economic and operational results indicate that excluding wind generation imposed a greater adaptation requirement under the investigated resource, cost, and grid conditions.

The PV/battery/grid S-OPT configuration achieved an LCOE of USD 0.133/kWh, approximately 1.5% lower than the USD 0.135/kWh reported in Ref. [55], while its renewable fraction of 43.6% was 11.5 percentage points lower than the 55.1% reported in that study. The close LCOE provides a useful cross-study reasonableness check, although direct numerical equivalence is not expected because of differences in load scale, tariff structure, component assumptions, renewable resources, demand profiles, and service assumptions. The comparison is therefore treated as a published benchmark rather than as direct validation.

3.5.3. Controlled Comparison and Planning Implications

To quantify the adaptation requirements directly, Table 8 reports the percentage reductions in annual unserved energy and CSF together with the percentage changes in PV, battery-bank size, converter capacity, and NPC from S-FIX to S-OPT. Positive component and NPC values indicate increases following adaptive re-optimization. The number of wind turbines remained unchanged for both wind-containing architectures and is therefore not repeated in Table 8.

Table 8 highlights the principal result of the controlled assessment. Adaptive re-optimization reduced annual unserved energy by approximately 73.2–97.2% across the three battery-containing architectures, but the physical changes required to obtain these improvements followed distinctly different patterns.

Wind/battery/grid achieved the largest reduction in unserved energy, 97.2%, with only minor increases in battery-bank size and converter capacity. In contrast, PV/wind/battery/grid reduced unserved energy by 73.2% but required increases of approximately 47% in both battery-bank size and converter capacity. PV/battery/grid achieved an 86.4% reduction through simultaneous expansion of PV generation, storage, and conversion capacity. Thus, fixed-design vulnerability and adaptation requirement represent different aspects of system performance.

The associated NPC increases of approximately 14–17% should be interpreted together with the substantial improvements in supply adequacy rather than simply as economic penalties. S-FIX represents operation of an unchanged baseline design under deteriorated grid conditions, whereas S-OPT represents an adaptively resized design. The higher S-

OPT NPC therefore reflects the lifecycle-cost implications of adaptation and the associated improvement in supply performance.

The most important finding is that the severity of fixed-design deterioration does not directly determine either the magnitude or the composition of the subsequent adaptation requirement. Wind/battery/grid experienced the greatest deterioration under S-FIX but required relatively little resizing. PV/wind/battery/grid retained substantially stronger fixed-design performance yet required much greater expansion of storage and conversion capacity. PV/battery/grid required simultaneous adaptation of generation, storage, and conversion capacity. These architecture-dependent responses would not be apparent from independently optimized severe-condition solutions alone.

From a planning perspective, the results therefore distinguish three separate considerations: the design that minimizes NPC under the original grid condition, the ability of that installed design to maintain performance if grid reliability deteriorates, and the physical and economic changes required for subsequent adaptation. The paired S-FIX–S-OPT assessment complements conventional scenario-specific optimization by explicitly quantifying the latter two aspects and thereby provides a more informative basis for planning grid-connected hybrid systems exposed to deteriorating grid reliability.

4. Sensitivity Analysis

4.1. Electricity Tariff Sensitivity

Figure 5 presents the joint influence of grid purchase price and sellback rate on NPC. NPC increased with the grid purchase tariff because a higher import price raised the annual cost of electricity obtained from the utility. Conversely, increasing the sellback tariff reduced NPC by increasing the financial value of exported renewable electricity.

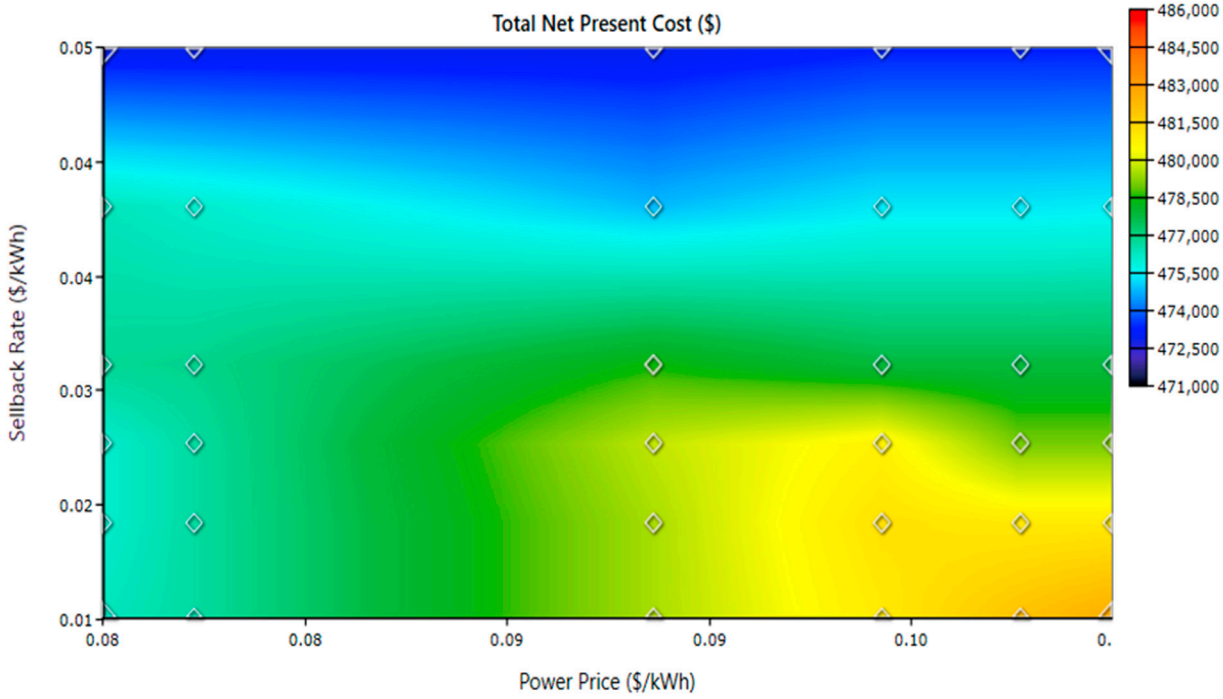

Figure 5. Joint sensitivity of NPC to grid purchase price and grid sellback rate.

The gradient of the response surface indicates that NPC was more sensitive to the purchase tariff than to moderate changes in the sellback rate. This behavior is consistent with the system's operating pattern because the domestic district remained a net grid importer, while the relatively low export tariff limited the financial contribution of surplus

renewable generation. More favorable sellback rates improved system economics but did not eliminate the dominant influence of the grid purchase price.

The observed nonlinearity should be interpreted as the combined effect of changing grid-related cash flows and possible discrete changes in optimized component sizing or dispatch. Consequently, tariff policy can materially affect project feasibility, particularly where import tariffs rise or stronger compensation for exported renewable electricity is introduced.

4.2. Sensitivity to Load Demand, Renewable Resources, and Initial Capital Cost

Table 9 examines the local sensitivity of the minimum-NPC solution to independent ±10% variations in electricity demand, solar irradiation, wind speed, and component initial capital cost. In all investigated cases, PV/wind/battery/grid remained the minimum-NPC architecture, indicating local stability of the architecture ranking within the tested deterministic ranges. Nevertheless, component sizing and economic performance varied appreciably, particularly in response to changes in electricity demand, wind speed, and component initial capital cost.

Table 9. Techno-economic, sizing, and supply-adequacy results of the deterministic ±10% sensitivity analysis.

Sensitivity Variable	Variation	Optimal Architecture	PV (kW)	EO20 Turbines	1 kWh LA Batteries	NPC ($)	LCOE ($/kWh)	Operating Cost ($/yr)	Resulting Initial Capital ($)	Renewable Fraction (%)	LPSP (%)	Annual Unserved Energy (MWh/yr)	Energy-Supply Availability (%)
Baseline case	0%	PV/wind/battery/grid	9.33	9	601	481,851	0.0711	17,379	376,510	73.8	0.0335	0.306	99.966
Load demand	−10%	PV/wind/battery/grid	8.88	8	525	431,562	0.0712	16,072	340,039	73.4	0.0358	0.294	99.964
Load demand	+10%	PV/wind/battery/grid	1.51	10	653	524,738	0.0705	19,414	414,184	73.4	0.0325	0.326	99.967
Solar irradiation	−10%	PV/wind/battery/grid	0.0691	9	583	477,048	0.0709	18,313	372,763	73	0.0369	0.337	99.963
Solar irradiation	+10%	PV/wind/battery/grid	0.238	9	590	478,618	0.0712	18,365	374,038	73	0.0353	0.322	99.965
Wind speed	−10%	PV/wind/battery/grid	1.5	10	624	514,381	0.0747	18,716	407,802	72.2	0.0396	0.361	99.960
Wind speed	+10%	PV/wind/battery/grid	0.254	9	585	454,091	0.0659	14,300	372,660	75.9	0.0346	0.316	99.965
Component initial capital cost	−10%	PV/wind/battery/grid	9.33	9	601	449,507	0.0663	17,315	350,904	73.8	0.0335	0.306	99.966
Component initial capital cost	+10%	PV/wind/battery/grid	1.85	9	596	513,967	0.0763	18,332	409,573	73.1	0.0336	0.307	99.966

Electricity demand had the strongest influence on the required system capacity and total lifecycle cost. Reducing the load by 10% decreased the optimal number of wind turbines from nine to eight and the number of battery units from 601 to 525. Consequently, the initial capital cost declined from $376,510 to $340,039, while NPC decreased by approximately 10.4%, from $481,851 to $431,562. Conversely, a 10% increase in demand required ten wind turbines and 653 battery units, raising the initial capital cost to $414,184 and NPC to $524,738, approximately 8.9% above the baseline value. Despite these changes, LCOE remained relatively stable, ranging from $0.0705 to 0.0712/kWh, because changes in annualized cost were accompanied by corresponding changes in supplied electricity.

The results show relatively weak sensitivity to solar-resource variation. A ±10% change in solar irradiation altered NPC by less than 1% relative to the baseline, while the renewable fraction remained close to 73%. This limited response is consistent with the relatively small optimized PV capacities and confirms that wind generation is the dominant renewable contributor in the selected architecture. The substantial changes in optimized PV capacity

despite only minor changes in NPC indicate the presence of economically close sizing solutions. Small changes in resource assumptions can therefore shift the minimum-NPC sizing solution without materially altering lifecycle cost.

Wind-speed variation produced a substantially stronger economic response than the corresponding solar-irradiation variation. A 10% reduction in wind speed increased the number of turbines from nine to ten and the battery requirement from 601 to 624 units. This raised the initial capital cost by approximately 8.3%, NPC by 6.8%, and LCOE by 5.1%, while reducing the renewable fraction from 73.8% to 72.2%. In contrast, a 10% increase in wind speed reduced NPC to $454,091 and LCOE to $0.0659/kWh, corresponding to reductions of approximately 5.8% and 7.3%, respectively. It also increased the renewable fraction to 75.9% and reduced annual operating cost by approximately 17.7%. Within the investigated ±10% range, wind-speed variation exerted a comparatively strong influence on component sizing, lifecycle cost, LCOE, and renewable fraction.

Changes in component initial capital cost produced an approximately symmetric but less-than-proportional response in lifecycle cost. A 10% reduction in capital cost lowered the resulting initial investment to $350,904, NPC to $449,507, and LCOE to $0.0663/kWh. Conversely, a 10% increase raised the initial capital requirement to $409,573, NPC to $513,967, and LCOE to $0.0763/kWh. These results correspond to changes of approximately ±6.7% in NPC, indicating that lifecycle economic performance remains sensitive to component-cost assumptions. Nevertheless, renewable fraction and annual unserved energy changed only marginally, indicating that capital-cost variation affects economic performance more strongly than technical adequacy.

From a supply-adequacy perspective, the sensitivity cases retained high energy-supply availability, with only small absolute variations in annual unserved energy and LPSP across the investigated deterministic ranges. Thus, the tested parameter variations affected system sizing and lifecycle economics more strongly than supply adequacy.

5. Conclusions

This study compared four grid-connected PV-, wind-, and battery-based architectures for residential-district electricity supply in Egypt under common technical, economic, and grid-outage assumptions. NPC was the sole optimization objective, while supply adequacy, renewable fraction, grid interaction, and grid-related operational CO_2 emissions were evaluated subsequently. Beyond conventional scenario-specific optimization, the study compared each baseline-optimal design operated unchanged under a common severe grid condition with the same architecture re-optimized under that condition. The main contribution is therefore a controlled comparative assessment that distinguishes baseline economic optimality, fixed-design performance under deteriorated grid reliability, and the requirements of adaptive redesign, rather than the development of a new optimization methodology.

Under the baseline condition, PV/wind/battery/grid was the minimum-NPC hybrid architecture, with an NPC of USD 481,851, an LCOE of USD 0.0711/kWh, a renewable fraction of 73.8%, and annual unserved energy of 0.306 MWh/yr. Although grid-only supply had a lower NPC of USD 369,414, the hybrid architecture reduced annual unserved energy by approximately 98.5% and grid-related operational CO_2 emissions by 65.0%, at an NPC premium of 30.4%. The results also showed that minimum lifecycle cost, maximum supply adequacy, highest renewable fraction, and lowest operational emissions were achieved by different architectures, emphasizing the trade-offs inherent in configuration selection.

The controlled severe-grid assessment provided the principal additional insight. For the three battery-containing architectures with complete adaptive results, re-optimization reduced annual unserved energy by 73.2–97.2%, but the required physical adaptation

differed substantially. Wind/battery/grid experienced the greatest fixed-design deterioration yet required only modest increases in battery and converter capacities, whereas PV/wind/battery/grid retained much stronger fixed-design performance but required approximately 47% increases in both storage and converter capacity. PV/battery/grid required simultaneous expansion of generation, storage, and conversion capacity. Among these complete adaptive cases, wind/battery/grid achieved the lowest NPC at USD 549,996, with PV/wind/battery/grid only approximately 0.63% higher. These findings demonstrate that the severity of fixed-design deterioration does not necessarily determine either the magnitude or the composition of the subsequent adaptation requirement.

Overall, the results show that baseline cost optimality, fixed-design performance, and adaptation requirements are distinct, architecture-dependent planning considerations. The deterministic ±10% sensitivity analysis retained PV/wind/battery/grid as the minimum-NPC architecture within the investigated ranges, indicating local stability of the ranking. The findings should nevertheless be interpreted within the study boundaries, particularly the use of one severe grid-availability profile, a single battery chemistry, constant tariffs, operational rather than full life-cycle emissions, and the absence of explicit land, siting, maximum-capacity, and grid-export constraints. Future work should therefore extend the analysis to probabilistic multi-year conditions, dynamic tariffs, alternative storage technologies, explicit site and interconnection constraints, life-cycle environmental assessment, and measured operational validation.

Author Contributions: Conceptualization, S.A., N.A.-H. and A.S.; methodology, S.A. and A.S.; software, S.A.; validation, S.A. and A.S.; formal analysis, S.A. and A.S.; investigation, S.A., N.A.-H. and A.S.; resources, S.A. and A.S.; data curation, S.A. and A.S.; writing—original draft preparation, S.A.; writing—review and editing, S.A., N.A.-H. and A.S.; visualization, S.A. and A.S.; supervision, S.A. and A.S.; project administration, S.A., N.A.-H. and A.S.; funding acquisition, S.A. and A.S. All authors have read and agreed to the published version of the manuscript.

Funding: This research received no external funding.

Data Availability Statement: The original contributions presented in this study are included in the article. For further inquiries, please contact the corresponding authors.

Conflicts of Interest: The authors declare no conflicts of interest.

References

1. Hasan, M.; Zarin, N.A.; Ahmed, M.R.; Farrok, O. Global Pathways for Hybrid Renewable Energy Systems: Challenges, Solutions, Policy, and Regulatory Frameworks. *Energy Convers. Manag. X* **2026**, *29*, 101534. [CrossRef]
2. Ghoudelbourk, S.; Ali, N.B.S.; Bayaud, M.; Yousfi, R. Energy Management Strategies for Hybrid Micro Grid System. In Proceedings of the 2023 IEEE 11th International Conference on Systems and Control (ICSC), Sousse, Tunisia, 18–20 December 2023; pp. 421–426. [CrossRef]
3. Nabipour-Afrouzi, H.; Wen Yii, S.H.; Ahmad, J.; Tabassum, M. Comprehensive Review on Appropriate Sizing and Optimization Technique of Hybrid PV-Wind System. In Proceedings of the 2018 IEEE PES Asia-Pacific Power and Energy Engineering Conference (APPEEC), Kota Kinabalu, Malaysia, 7–10 October 2018; pp. 364–369. [CrossRef]
4. T, G.; Kesavan, J.; Srividhya, P.K.; Ramkumar, P. Towards Greener Horizons: A Comprehensive Review of Energy Auditing in Hybrid Solar and Wind Systems. *Interactions* **2024**, *245*, 221. [CrossRef]
5. Gaurav, A.; Tyagi, A.; Jha, S.K.; Kumar, B. Assessment Using MCDM Approach of Renewable Hybrid Energy System with Hydrogen Production Capability. *Int. J. Hydrogen Energy* **2025**, *137*, 448–460. [CrossRef]
6. Basnet, S.; Deschinkel, K.; Le Moyne, L.; Cécile Péra, M. A Review on Recent Standalone and Grid Integrated Hybrid Renewable Energy Systems: System Optimization and Energy Management Strategies. *Renew. Energy Focus* **2023**, *46*, 103–125. [CrossRef]
7. Hassan, R.; Das, B.K.; Al-Abdeli, Y.M. Investigation of a Hybrid Renewable-Based Grid-Independent Electricity-Heat Nexus: Impacts of Recovery and Thermally Storing Waste Heat and Electricity. *Energy Convers. Manag.* **2022**, *252*, 115073. [CrossRef]
8. Zhao, K.; Zheng, K.; Shen, C.; Ge, J. Configuration Optimization and Performance Analysis of Hybrid PV/Wind Systems in Building Groups. *J. Build. Eng.* **2024**, *97*, 110696. [CrossRef]

9. Ibáñez-Rioja, A.; Puranen, P.; Järvinen, L.; Kosonen, A.; Ruuskanen, V.; Ahola, J.; Koponen, J. Simulation Methodology for an Off-Grid Solar–Battery–Water Electrolyzer Plant: Simultaneous Optimization of Component Capacities and System Control. *Appl. Energy* **2022**, *307*, 118157. [CrossRef]
10. Qureshi, Z.u.A.; Kazmi, S.A.A.; Mushtaq, S.; Anwar, M. An Integrated Assessment Framework of Renewable Based Microgrid Deployment for Remote Isolated Area Electrification across Different Climatic Zones and Future Grid Extensions. *Sustain. Cities Soc.* **2024**, *101*, 105069. [CrossRef]
11. Thirunavukkarasu, M.; Sawle, Y.; Lala, H. A Comprehensive Review on Optimization of Hybrid Renewable Energy Systems Using Various Optimization Techniques. *Renew. Sustain. Energy Rev.* **2023**, *176*, 113192. [CrossRef]
12. Vishnu Dharssini, A.C.; Charles Raja, S. Three-Tier Integrated Demand-Supply Energy Management for Optimized Energy Usage in Institutional Building. *Energy Build.* **2024**, *318*, 114439. [CrossRef]
13. Subramaniam, U.; Vavilapalli, S.; Padmanaban, S.; Blaabjerg, F.; Holm-Nielsen, J.B.; Almakhles, D. A Hybrid PV-Battery System for ON-Grid and OFF-Grid Applications—Controller-In-Loop Simulation Validation. *Energies* **2020**, *13*, 755. [CrossRef]
14. Chedid, R.; Sawwas, A.; Fares, D. Optimal Design of a University Campus Micro-Grid Operating under Unreliable Grid Considering PV and Battery Storage. *Energy* **2020**, *200*, 117510. [CrossRef]
15. Azerefegn, T.M.; Bhandari, R.; Ramayya, A.V. Techno-Economic Analysis of Grid-Integrated PV/Wind Systems for Electricity Reliability Enhancement in Ethiopian Industrial Park. *Sustain. Cities Soc.* **2020**, *53*, 101915. [CrossRef]
16. Lin, X.M.; Kireeva, N.; Timoshin, A.V.; Naderipour, A.; Abdul-Malek, Z.; Kamyab, H. A Multi-Criteria Framework for Designing of Stand-Alone and Grid-Connected Photovoltaic, Wind, Battery Clean Energy System Considering Reliability and Economic Assessment. *Energy* **2021**, *224*, 120154. [CrossRef]
17. Ahmed, M.R.; Das, B.K.; Tushar, M.S.H.K. Investigation of a Grid-Integrated Hybrid Energy System for Residential and Electric Vehicle (3-Wheeler) Loads under Schedule Grid Outage. *Alex. Eng. J.* **2023**, *80*, 241–258. [CrossRef]
18. Ahmed, R.; Hasan, N.; Shezan, S.A.; Ishraque, F.; Das, B.K.; Tushar, S.H.K. Assessment of a Grid-Connected Microgrid for Suburban Areas and EV Loads with Battery Storage during Planned Grid Outages Using DIgSILENT Powerfactory. *Electr. Eng.* **2025**, *107*, 15069–15098. [CrossRef]
19. Adetoro, S.A.; Olatomiwa, L.; Tsado, J.; Dauda, S.M. Techno-Economic and Environmental Impact Assessment of a Hybrid Renewable Energy System Employing an Enhanced Combined Dispatch Strategy. *Green Energy Resour.* **2023**, *1*, 100044. [CrossRef]
20. Grant, E.; Clark, C.E. Hybrid Power Plants: An Effective Way of Decreasing Loss-of-Load Expectation. *Energy* **2024**, *307*, 132245. [CrossRef]
21. Shahnazian, F.; Das, K.; Yan, R.; Sorensen, P.E. Hybrid Power Plant Control to Enhance Voltage Stability in Weak Grid. *Int. J. Electr. Power Energy Syst.* **2025**, *172*, 111070. [CrossRef]
22. Founti, M.; Nikolaidis, G.N.; Thango, B.A.; Obokoh, L. Techno-Economic Analysis of Hybrid Renewable Energy Systems for Power Interruptions: A Systematic Review. *Eng* **2024**, *5*, 2108–2156. [CrossRef]
23. Emmanuel, M.; Doubleday, K.; Cakir, B.; Marković, M.; Hodge, B.M. A Review of Power System Planning and Operational Models for Flexibility Assessment in High Solar Energy Penetration Scenarios. *Sol. Energy* **2020**, *210*, 169–180. [CrossRef]
24. Gasser, P.; Lustenberger, P.; Cinelli, M.; Kim, W.; Spada, M.; Burgherr, P.; Hirschberg, S.; Stojadinovic, B.; Sun, T.Y. A Review on Resilience Assessment of Energy Systems. *Sustain. Resilient Infrastruct.* **2021**, *6*, 273–299. [CrossRef]
25. Alharbi, A.M.; Zaki Diab, A.A. Enhancing Off-Grid Hybrid Renewable Energy Systems through Multi-Objective Optimization with Pareto Front Analysis. *Energy* **2026**, *351*, 140728. [CrossRef]
26. Khan, W.A.; Pakseresht, A.; Chua, C.; Yavari, A. Energy Resilience and Decarbonization via Hybrid Renewable Energy Systems: A Techno-Economic Study. *Int. J. Hydrogen Energy* **2026**, *217*, 153765. [CrossRef]
27. Zhang, Z.; Qin, H.; Li, J.; Liu, Y.; Yao, L.; Wang, Y.; Wang, C.; Pei, S.; Zhou, J. Short-Term Optimal Operation of Wind-Solar-Hydro Hybrid System Considering Uncertainties. *Energy Convers. Manag.* **2020**, *205*, 112405. [CrossRef]
28. Khan, A.; Bressel, M.; Davigny, A.; Abbes, D.; Ould Bouamama, B. Comprehensive Review of Hybrid Energy Systems: Challenges, Applications, and Optimization Strategies. *Energies* **2025**, *18*, 2612. [CrossRef]
29. Korovushkin, V.; Boichenko, S.; Artyukhov, A.; Ćwik, K.; Wróblewska, D.; Jankowski, G. Modern Optimization Technologies in Hybrid Renewable Energy Systems: A Systematic Review of Research Gaps and Prospects for Decisions. *Energies* **2025**, *18*, 4727. [CrossRef]
30. Uwaezuoke, C.T.; Nwulu, N.I. Hybrid Renewable Energy for Agriculture: Review of Optimising Power Dispatch and Reliability Analysis. *Energy Nexus* **2026**, *21*, 100679. [CrossRef]
31. Pandyaswargo, A.H.; Wibowo, A.D.; Onoda, H. Socio-Techno-Economic Assessment to Design an Appropriate Renewable Energy System for Remote Agricultural Communities in Developing Countries. *Sustain. Prod. Consum.* **2022**, *31*, 492–511. [CrossRef]
32. Makai, L.; Popoola, O. A Review of Micro-Hybrid Energy Systems for Rural Electrification, Challenges and Probable Interventions. *Renew. Energy Focus* **2025**, *53*, 100687. [CrossRef]
33. Faraji, H.; Hemmati, R. A Novel Resilient Concept for District Energy System Based on Central Battery and Decentral Hybrid Generating Resources. *Int. J. Energy Res.* **2022**, *46*, 11925–11942. [CrossRef]

34. Deevela, N.R.; Singh, B.; Kandpal, T.C. Optimization and Economic Analysis of Solar PV Based Hybrid System for Powering Base Transceiver Stations in India. *Energy* **2023**, *283*, 129160. [CrossRef]
35. Salehi, M.; Khanali, M.; Ghasemi-Mobtaker, H. Techno-Economic Analysis of Renewable Hybrid System Microgrids for Minimizing Grid Power Outages in Residential Areas. *Clean. Eng. Technol.* **2025**, *25*, 100924. [CrossRef]
36. Shahverdian, M.H.; Sohani, A.; Zamani Pedram, M.; Sayyaadi, H. An Optimal Strategy for Application of Photovoltaic-Wind Turbine with PEMEC-PEMFC Hydrogen Storage System Based on Techno-Economic, Environmental, and Availability Indicators. *J. Clean. Prod.* **2023**, *384*, 135499. [CrossRef]
37. Mazzeo, D.; Matera, N.; De Luca, P.; Baglivo, C.; Congedo, P.M.; Oliveti, G. A Literature Review and Statistical Analysis of Photovoltaic-Wind Hybrid Renewable System Research by Considering the Most Relevant 550 Articles: An Upgradable Matrix Literature Database. *J. Clean. Prod.* **2021**, *295*, 126070. [CrossRef]
38. Nazir, K.; Nobi Siam, M.M.; Islam, A.T.M.S. Techno-Economic Feasibility and Sensitivity Analysis of Stand-Alone Hybrid Renewable Energy System: A Case Study at University Campus in Bangladesh. *Energy Convers. Manag. X* **2026**, *29*, 101514. [CrossRef]
39. Jafari, M.; Sayyaadi, H. Optimal Off-Grid Electricity Supply for a Residential Complex Using Water-Energy-Economic-Environmental Nexus. *Energy Convers. Manag. X* **2025**, *26*, 100998. [CrossRef]
40. Baghel, N.; Manjunath, K.; Kumar, A. Techno-Economic Analysis of Hybrid Renewable Power Generation System under Different Climatic Zones in India. *Electr. Eng.* **2025**, *107*, 8465–8480. [CrossRef]
41. Ozturk, Z.; Terkes, M.; Demirci, A. Optimal Planning of Hybrid Power Systems under Economic Variables and Different Climatic Regions: A Case Study of Türkiye. *Renew. Energy* **2024**, *232*, 121029. [CrossRef]
42. Tufail, S.; Riggs, H.; Sarwat, A. Techno-Economic and Environmental Assessment of Photovoltaic–Battery Microgrids across Diverse U.S. States. *Energy Convers. Manag. X* **2026**, *30*, 101668. [CrossRef]
43. Abdelhady, S. Techno Economic Assessment and Comparative Study of Photovoltaic (PV) and High Concentration PV (HCPV) Large Scale Power Systems under Different Scenarios: Sensitivity Analysis. *Results Eng.* **2025**, *26*, 105653. [CrossRef]
44. Abdelhady, S.; Al-Hinai, N.; Al Kindi, M.; Gultekin, H.; Shaban, A. Techno-Economic Assessment of Offshore Wind Energy-to-Electricity and Hydrogen Production Systems in Egypt and Oman: Insights for the MENA Region. *Energies* **2026**, *19*, 129. [CrossRef]
45. Emam, M.M.; El-Sattar, H.A.; Houssein, E.H.; Kamel, S. Optimized Design and Integration of an Off-Grid Solar PV-Biomass-Battery Hybrid Energy System Using an Enhanced Educational Competition Algorithm for Cost-Effective Rural Electrification. *J. Energy Storage* **2025**, *120*, 116381. [CrossRef]
46. Abouaiana, A. Rural Energy Communities as Pillar towards Low Carbon Future in Egypt: Beyond COP27. *Land* **2022**, *11*, 2237. [CrossRef]
47. Tazay, A.F.; Ibrahim, A.M.A.; Noureldeen, O.; Hamdan, I. Modeling, Control, and Performance Evaluation of Grid-Tied Hybrid Pv/Wind Power Generation System: Case Study of Gabel El-Zeit Region, Egypt. *IEEE Access* **2020**, *8*, 96528–96542. [CrossRef]
48. Diab, F.; Lan, H.; Zhang, L.; Ali, S. An Environmentally Friendly Factory in Egypt Based on Hybrid Photovoltaic/Wind/Diesel/Battery System. *J. Clean. Prod.* **2016**, *112*, 3884–3894. [CrossRef]
49. Aziz, A.S.; Tajuddin, M.F.N.; Zidane, T.E.K.; Su, C.L.; Mas'ud, A.A.; Alwazzan, M.J.; Alrubaie, A.J.K. Design and Optimization of a Grid-Connected Solar Energy System: Study in Iraq. *Sustainability* **2022**, *14*, 8121. [CrossRef]
50. Bakht, M.P.; Salam, Z.; Gul, M.; Anjum, W.; Kamaruddin, M.A.; Khan, N.; Bukar, A.L. The Potential Role of Hybrid Renewable Energy System for Grid Intermittency Problem: A Techno-Economic Optimisation and Comparative Analysis. *Sustainability* **2022**, *14*, 14045. [CrossRef]
51. Al-Khaykan, A.; Al-Kharsan, I.H.; Ali, M.O.; Alrubaie, A.J.; Fakhruldeen, H.F.; Counsell, J.M. Impact of Multi-Year Analysis on the Optimal Sizing and Control Strategy of Hybrid Energy Systems. *Energies* **2023**, *16*, 110. [CrossRef]
52. Manoo, M.U.; Shaikh, F.; Kumar, L.; Mustapa, S.I. Comparative Investigation of On-Grid and Off-Grid Hybrid Energy System for a Remote Area in District Jamshoro of Sindh, Pakistan. *Urban Sci.* **2023**, *7*, 63. [CrossRef]
53. Akindeji, K.T.; Ewim, D.R.E. Economic and Environmental Analysis of a Grid-Connected Hybrid Power System for a University Campus. *Bull. Natl. Res. Cent.* **2023**, *47*, 75. [CrossRef]
54. Sanda, M.G.; Emam, M.; Ookawara, S.; Hassan, H. Techno-Enviro-Economic Evaluation of on-Grid and off-Grid Hybrid Photovoltaics and Vertical Axis Wind Turbines System with Battery Storage for Street Lighting Application. *J. Clean. Prod.* **2025**, *491*, 144866. [CrossRef]
55. Abdelhady, S.; Shaban, A. Comprehensive Techno-Economic and Environmental Comparison with Sensitivity Analysis of Optimized Hybrid Energy Systems for Residential Prosumers. *Sustainability* **2026**, *18*, 6478. [CrossRef]
56. HOMER. Welcome to HOMER. Available online: https://support.ul-renewables.com/homer-manuals-pro/index.html (accessed on 30 July 2025).
57. Abdelhady, S.; Shaban, A. A Simulation Modeling Approach for the Techno-Economic Analysis of the Integration of Electric Vehicle Charging Stations and Hybrid Renewable Energy Systems in Tourism Districts. *Appl. Sci.* **2024**, *14*, 4525. [CrossRef]

58. Navas, S.J.; Cabello González, G.M.; Pino, A.; Pino, F.J. Integration of Microgrids in Chemical Industries with Hydrogen as a Byproduct: Styrene Production Case Study. *Int. J. Hydrogen Energy* **2024**, *59*, 947–957. [CrossRef]
59. Abdelhady, S. Techno-Economic Study and the Optimal Hybrid Renewable Energy System Design for a Hotel Building with Net Zero Energy and Net Zero Carbon Emissions. *Energy Convers. Manag.* **2023**, *289*, 117195. [CrossRef]
60. Egyptera Rules of Net Metering System in Egypt. Available online: https://egyptera.org/ar/RegulatedRules.aspx (accessed on 11 March 2026).
61. Central Bank of Egypt. Available online: https://www.cbe.org.eg/en/ (accessed on 18 November 2025).

Disclaimer/Publisher's Note: The statements, opinions and data contained in all publications are solely those of the individual author(s) and contributor(s) and not of MDPI and/or the editor(s). MDPI and/or the editor(s) disclaim responsibility for any injury to people or property resulting from any ideas, methods, instructions or products referred to in the content.